



# A mathematical model to predict the effect of electrospinning processing parameters on the morphological characteristic of nano-fibrous web and associated filtration efficiency



Naghm Ismail<sup>a</sup>, Fouad Junior Maksoud<sup>b</sup>, Nesreen Ghaddar<sup>a,\*</sup>, Kamel Ghali<sup>a</sup>, Ali Tehrani-Bagha<sup>b</sup>

<sup>a</sup> Mechanical Engineering Department, American University of Beirut, P.O. Box 11-0236, Beirut 1107-2020, Lebanon

<sup>b</sup> Department of Chemical and Petroleum Engineering, American University of Beirut, PO Box 11-236, Beirut 1107-2020, Lebanon

## ARTICLE INFO

### Keywords:

Nano-fibrous web  
Electrospinning  
Morphological properties  
Filtration efficiency

## ABSTRACT

A robust simplified method was developed to study the effect of electrospinning processing parameters on the morphological properties of electrospun nano-fibrous web, its air permeability, and filtration efficiency against aerosol particles. The developed predictive model related the electrospinning processing parameters to the nano-fibrous web properties. The model was validated experimentally and then is used to study the effect of each electrospinning processing parameters (flow rate, electric field, concentration, and time of electrospinning) on the nano-fibrous web properties. For example, it is shown that only 20 min of electrospinning is able to reduce the air permeability by 66% while one hour of electrospinning coating time is able to increase the filtration efficiency to reach 100% for a range of aerosol particle diameters from 300 to 1000 nm. The validated systematic model is used for developing design charts that allow the determination of the desired air permeability and the filtration performance of the nano-fibrous web from the electrospinning parameters and vice versa within a wide range of feasible processing parameters and fiber diameters.

## 1. Introduction

Over the last two decades, the rapid development of the nanotechnology resulted in great progress, not only in the preparation of nanofibers, but also in their functional applications (Fang, Wang, & Li, 2011). Currently, the most interesting applications are identified in the following functional areas: biomedical, energy harvest and storage, and environmental protection (Fang et al., 2011). The environmental protection is considered of great importance since current environmental problems have serious negative impacts on human health (Haines, Kovats, Campbell-Lendrum, & Corvalan, 2006). Nanofibers are expected to be used in the filtration of pollutant substances from air or liquid due to their high specific surface area (Barhate & Ramakrishna, 2007). Furthermore, the high porosity, the low basis weight, and the small pore size make the nanofibers appropriate to be used in garments for protective clothing (Lee & Obendorf, 2007). Another important feature of nanofibers in protective garment is its high air permeability compared to most conventional protective clothing material currently available (Lee & Obendorf, 2007).

A number of processing techniques have been used to prepare polymeric nanofibers (Huang, Zhang, Kotaki, & Ramakrishna, 2003). Among these techniques is the electrospinning process which is a simple and convenient technique for production of

\* Corresponding author.

E-mail address: [farah@aub.edu.lb](mailto:farah@aub.edu.lb) (N. Ghaddar).

<b>Nomenclature</b>		$v_f$	length of fiber deposited per time (m/s)
$AP$	air permeability (m/s)	$w$	basis weight (g/m <sup>2</sup> )
$C$	polymer concentration	$\bar{z}$	thickness (m)
$C_r$	correction factor	<i>Greek symbols</i>	
$C_c$	Cunningham slip correction factor	$\alpha$	solidity
$C_d$	downward concentration of the aerosol particles	$\mu$	viscosity (N s/m <sup>2</sup> )
$C_u$	upward concentration of the aerosol particles	$\eta$	filter collection efficiency
$d_f$	fiber diameter (m)	$\eta_{\Sigma}$	total single fiber efficiency
$E$	electric field (V/m)	$\eta_D$	single fiber efficiency by diffusion
$I$	electric current (A)	$\eta_{DR}$	single fiber efficiency by enhanced interception-diffusion
$k_b$	Boltzman constant	$\eta_R$	single fiber efficiency by interception
$kn$	Knudsen number	$\gamma$	surface tension coefficient (N/m)
$ku$	Kuwabura number	$\lambda$	mean free path of air molecules (m)
$m,f$	mass deposition rate of fibers (kg/s)	$x$	characteristic length
$N_f$	number of fibers	$\Delta P$	standard pressure drop for testing fabric (124.5 Pa)
$p$	porosity	$\rho$	density of the solution (kg/m <sup>3</sup> )
$pe$	Peclet number	$\rho_b$	bulk density of the nano-fibrous web (kg/m <sup>3</sup> )
$Q$	volumetric mass flow rate (m <sup>3</sup> /s)	$\rho_f$	density of the fiber (kg/m <sup>3</sup> )
$R$	interception number	$\rho_p$	density of the aerosol particle (kg/m <sup>3</sup> )
$R_c$	radius of collector (m)	$\chi$	characteristic length
$Stk$	particle Stokes number	$\omega$	rotation rate (rd./s)
$T$	temperature (K)	$\varepsilon$	permittivity of air
$t_e$	time of electrospinning (s)		
$u_0$	face velocity (m/s)		
$v_T$	deposition velocity (m/s)		

polymeric nanofibers and nanocomposites (Lee & Obendorf, 2007). It is based on accelerating a polymer solution in an electric field between a charged nozzle and a ground collector (Shin, Hohman, Brenner, & Rutledge, 2001). The electrospun nanofibers are usually deposited on a high permeable and porous substrate covering the collector of the electrospinning device (Lee & Obendorf, 2007). The result is a nano-fibrous web of high porosity, large surface-to-volume ratio, light weight, relatively high air permeability and small pore size.

The small pore size characteristic of the nano-fibrous web results in improved air filtration performance. Chattopadhyay, Hatton, and Rutledge (2015) studied the aerosol filtration of electrospun cellulose acetate filters with different mean fiber diameters and compared the results with two conventional filters (glass fiber and microfiber filters). Kuo, Bruno, and Wang (2014) investigated the performance of ultrafine nanofibers against nanoparticles and showed that this type of filter is advantageous especially when high filtration efficiency is required at low weight. Indeed, the air filtration performance of the electrospun nano-fibrous web is related to the electrospinning processing parameters, the air face velocity, and the aerosol particle diameter. The properties of electrospun fibers can be manipulated by varying the processing parameters of electrospinning such as the polymer concentration, the electric field, the time of electrospinning, and the volumetric flow rate Leung, Hung, and Yuen (2010); Pai, Boyce, and Rutledge (2011)). In addition, the fiber diameter, the fiber thickness, and the porosity affect the filtration performance of the filter as well as its air permeability at different air face velocity (Abuzade, Zadhouseh, & Gharehaghaji, 2012; Leung et al., 2010).

The electrospun nano-fibrous web used in protective garments is recommended to have a desirable rate of air permeability to improve clothing breathability which can be achieved by optimizing the electrospinning process (Abuzade et al., 2012). Usually, the optimization method to set electrospinning process parameters reported in literature has been dependent on empirical methods (Faccini, Vaquero, & Amantia, 2012). However, the use of a modeling approach of electrospinning process to predict nano-fibrous web morphology (fiber diameter, porosity, thickness), air permeability and filtration efficiency would serve as an important design tool in such processes.

Many researchers have developed models that estimate the fiber diameter based on the polymer solution properties and the electrospinning effective parameters (Taylor, 1969; Feng, 2002; Hohman, Shin, Rutledge, & Brenner, 2001; Yarin, 2011). Some of these models were limited to a single electrospinning stage and did not model the whole electrospinning process (Taylor 1969; Feng 2002). Other models were complex and necessitated a high computational cost (Yarin, 2011). Fridrikh, Jian, Brenner, and Rutledge (2003) derived a simplified model that related the processing parameters to the final fiber diameter. This model was recently used by Ismail, Maksoud, Ghaddar, Ghali, and Tehrani (2016) who developed a combined accurate mathematical model that covers both the stable and the unstable stages of electrospinning to predict the fiber diameter.

The porosity of the nano-fibrous web, which is a function of the fiber diameter and the web thickness, can also be estimated by a direct measurement or a theoretical model. The bulk density and porosity of the nano-fibrous web can be measured by a number of techniques such as the Scanning Electron Microscope (SEM) and the weighting technique (Ma, Kotaki, Yong, He, & Ramakrishna, 2005). By considering the mat as quantized planes of overlapping fibers and creating a randomly oriented fibers grid, one can estimate the porosity of the web by a theoretical model (Lowery, 2009).

The nano-fibrous web thickness is a necessary parameter for estimating the porosity of a nano-fibrous web. Scanning Electron Microscope and film thickness measurement gage can be used for measuring the thickness of the webs (Boppa, 2009). Theoretically, the thickness can be predicted assuming that no losses of polymer occur during the electrospinning process by applying the mass conservation of polymer (Kwankhao, Ulbricht, & Gutmann, 2013). Wang, Maze, Tafreshi, and Pourdeyhimi (2007) and Tafreshi, Rahman, Jaganathan, Wang, and Pourdeyhimi (2009) modelled the air permeability of fibrous media. Nevertheless, their modeling approach cannot be adopted to predict the air permeability in the nanometer scale because it does not take into account the slip effect of the flow around a nanofiber. Hosseini and Tafreshi (2010) incorporated the slip condition effect on modeling the air permeability and developed an analytical approach that was corrected for the existing permeability expressions to fit the nano-fibrous media. Most filtration studies (Yun, Hogan, Matsubayashi, Kawabe, Iskandar, & Okuyama, 2007; Hill, Ghee, Kaufman, & Dhaniyala, 2013) are based on the classical single fiber efficiency theories (Kirsh, Stechkina, & Fuchs, 1975; Davies, 1973). When investigating the filtration of the nano-fibrous web, the theory of Kirsh et al. (1975) was adopted where the fiber collection efficiency due to diffusion, interception and impaction of particles were evaluated allowing for the gas slip near the fiber surface. A combination of these models would be essential for assessing the effect of the electrospinning processing parameters on the morphological properties and the filtration performance of the electrospun nano-fibrous web.

The aim of this study is to present a modeling method to study the effect of processing parameters on the properties and air filtration performance of nano-fibrous webs. Thus, a systematic simplified model is developed to relate the electrospinning processing parameters to (i) the penetration of aerosol particles through the electrospun nanofiber for a range of particle diameter and to (ii) the air permeability of the electrospun nanofiber that usually depends on the porosity and the thickness of the electrospun nanofiber. The electrospun fiber diameter will be predicted using the recently developed model of Ismail et al. (2016). Furthermore, the porosity of the web will be estimated using a numerical model based on randomly distributed fibers model (Lowery, 2009). The thickness and porosity of the nano-fibrous webs will be used in finding the air permeability (Hosseini & Tafreshi, 2010). Finally, the analytical expressions for the filtration or the penetration efficiency will be used to assess the filter performance (Kirsh et al., 1975). The morphological properties and the filtration efficiency of the nano-fibrous webs obtained by the modeling approach will be experimentally validated.

The contribution of this work to the field is in the development of design charts that relate the filtration efficiency and the air permeability to the electrospinning processing parameters. These design charts allow any researcher to know the appropriate

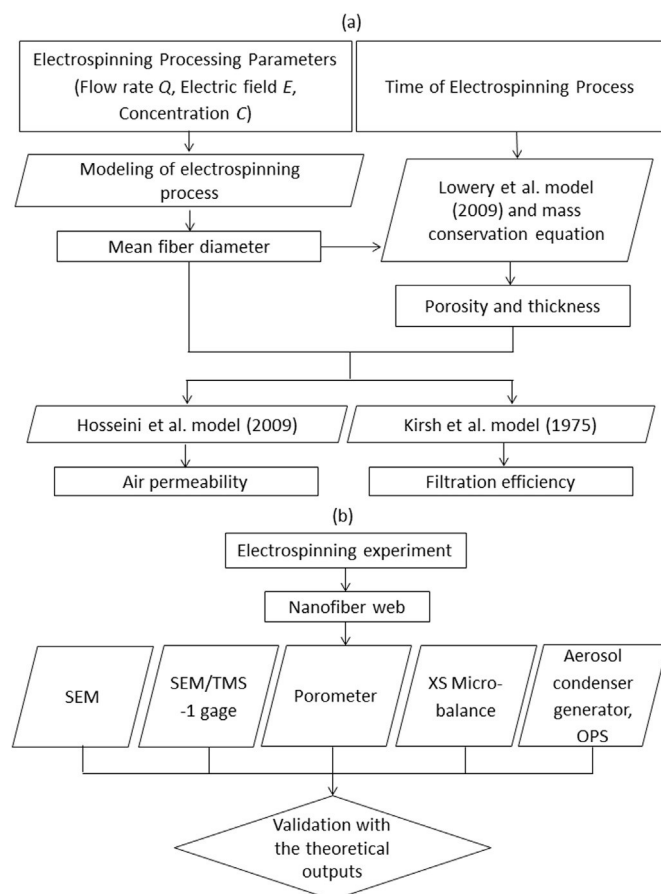


**Fig. 1.** Flow chart of the research methodology in (a) the theoretical model and (b) the experimental validation.

processing parameters of electrospinning process to produce the electrospun nano-web of desirable air permeability and filtration efficiency and vice versa. Therefore, this method will reduce the time and material costs of the electrospinning experimental trials for reaching sought characteristics of the nano-fibrous web.

## 2. Research methodology

We have recently developed a theoretical model (Ismail et al., 2016) in which the electrospinning processing parameters are used to find the final fiber diameter of electrospun nanofiber. The model covered the two connected stages of electrospinning: stable and unstable jets. The electrospinning processing parameters are mainly: the volumetric flow rate  $Q$ , the electric field  $E$ , and the polymer concentration in the solution  $C$ . The porosity of the nano-fibrous web is found by using the numerical model developed by Lowery (2009) in which the mat is treated as quantized planes of overlapping fibers. Other morphological properties like thickness  $\bar{z}$  and basis weight  $w$  are then computed by using mass conservation assuming that no polymer losses occurred (Kwankhao et al., 2013). On the other hand, the morphological properties are used to determine the air permeability of electrospun nanofiber by adopting an accurate model that predicts the air permeability of the fibrous materials made up of nanofibers taking into account the effect of slip flow (Hosseini & Tafreshi 2010). After exploring the morphological properties of the nano-fibrous web, the filtration efficiency can be obtained from the classical filtration theory (Kirsh et al., 1975) at a range of aerosol particle diameter. Finally, a series of experiments is conducted to validate the predictions of porosity, thickness, filtration efficiency, and air permeability. The performed experiments start by the fabrication of the electrospun nano-fibrous web using the electrospinning device, afterwards; the porosity and the thickness of the electrospun nano-fibrous web are measured using microbalance and SEM device respectively. Moreover, the air permeability is measured by a capillary flow porometer. Finally, the filtration efficiency is measured by performing an experiment on the electrospun nano-fibrous web through generating aerosol particles and measuring their upstream and downstream concentrations. Fig. 1 shows the methodology of (a) the theoretical modeling and (b) the validation strategy.

### 2.1. Mathematical formulation

The fiber diameter is theoretically predicted using our recent model (Ismail et al., 2016) that couples the two electrospinning stages to relate the electrospinning parameters to the final fiber diameter. The fiber diameter and the time of electrospinning are then used to estimate the thickness and porosity which are necessary to accurately estimate the air permeability and the filtration efficiency of the nano-fibrous web.

#### 2.1.1. Fiber diameter prediction

The model of Ismail et al. (2016) is used in the current work to predict the nano-fibrous web fiber diameter where the behavior of the electrospun polymer is obtained by solving the electro-hydrodynamics equations including the mass, momentum, charge conservation and Coulomb's law inside the fluid jet in the initial stable jet region to the final unstable jet region. The inputs for the governing equations are the solution properties, and the processing parameters. The solution properties are mainly related to the polymer, selected solvent and the polymeric concentration  $C$  in the solution. The processing parameters are related to the electrospinning process such as the flow rate  $Q$ , the electric field  $E$ , and the initial radius of the jet assumed equal to the nozzle radius. The final fiber diameter is deduced by assuming that at the final stage of electrospinning, the competition of forces is between the surface tension and the electrostatic repulsion forces:

$$d_f = C^{0.5} \left( \frac{\gamma \bar{e}}{I^2} \frac{2}{\pi (2 \ln \chi - 3)} \right)^{1/3} \quad (1)$$

where  $\gamma$  is the surface charge density of the jet,  $\bar{e}$  is the dielectric permittivity of the jet,  $I$  is the electric current estimated by the model using the correlation of Bhattacharjee, Schneider, Brenner, McKinley and Rutledge (2010). The model of Ismail et al. (2016) covers the complete electrospinning process by coupling the properties of the stable jet to the unstable jet region. This coupling between the stable and the unstable jet allows the determination of the characteristic length  $\chi$  defined as the ratio of the bending instability wavelength to the stable radius of the jet. The wavelength is estimated from the fastest growing mode of the spinning jet that leads to the maximum thinning, and it is mainly a function of the jet viscosity, the surface charge density and the jet radius of the stable jet. These stable jet properties are obtained from modeling the stable jet region based on the conservation equations of mass, momentum, and electric charges, as well as additional electro-hydrodynamic equations. The adopted model of Ismail et al. (2016) accurately predicts the final fiber diameter of electrospinning which is an essential parameter for estimating the morphological properties of electrospun nano-fibrous web. The applicability of the model of Ismail et al. (2016) is limited to electrospinning processes at low relative humidity (less than 40%) since higher relative humidity leads to the formation of beads and hence increases the fiber diameter (Ballengee & Pintauro, 2011).

#### 2.1.2. Morphological properties of the electrospun nanofiber

The morphological properties of the electrospun nano-fibrous web are mainly related to the fiber diameter and the basis weight (i.e., the mass of the fiber per unit area). The later increases by prolonging the electrospinning time. The morphological properties described in this section are the porosity, the thickness, and the air permeability.

**2.1.2.1. Porosity.** In order to theoretically predict the porosity of the electrospun nanofiber, the algorithm of Lowery (2009) is

adopted. This algorithm is based on treating the mat as quantized planes of overlapping fibers and creating a randomly oriented fibers grid. The algorithm is converted to a numerical model written in Matlab language. The input variables to the numerical model are the sample dimensions of the deposition area, the fiber diameter, and the number of fibers generated (Lowery, 2009). The output variables of this numerical model include the number of pores, the mass density vector defined as the number of fibers localized in each node of the studied mat, and the overall porosity of the mat. Before executing the simulation, the number of fibers is predicted depending on the processing parameters. The mass deposition rate of fibers  $\dot{m}_f$  is calculated as a function of the solution volumetric flow rate  $Q$ , the solution density  $\rho$ , and the polymer concentration  $C$  as follows:

$$\dot{m}_f = Q \rho C \quad (2)$$

Using the electrospun fiber diameter computed from Eq. (1), the length of fiber deposited per time is given by (Lowery, 2009):

$$v_f = \frac{4 \dot{m}_f}{\rho_f \pi d_f^2} \quad (3)$$

where  $\rho_f$  is the fiber density which is assumed equal to the polymer density.

It is important to note that the rate of deposition of the fiber on the rotating collector is related to the rotation speed and the collector radius (Lowery, 2009) as follows:

$$v_T = 2\pi R_c \omega \quad (4)$$

where  $v_T$  is the velocity of the deposition point on the rotating collector,  $R_c$  is the radius of the rotating collector, and  $\omega$  is the rotation rate. Finally, the number of fibers during a single rotation is computed by dividing the length of the fiber deposited per time to the rate of fiber deposition. Thus the total number of fibers  $N_f$  for the complete electrospinning process is calculated as

$$N_f = \frac{v_f}{v_T} 2\pi \omega t_e \quad (5)$$

where  $t_e$  is the electrospinning process time. After computing the number of fibers generated during the electrospinning process, a small sample of the nanofiber mat is chosen and its dimensions are used as an input to the numerical model. The fiber diameter is computed using Eq. (1), and the number of fibers generated for this sample is predicted by multiplying the total number of fibers by the geometrical ratio of the sample to the total collector surface area. In order to compute the porosity  $p$ , the numerical model counts the number of void nodes unoccupied by the fibers over the total number of nodes.

**2.1.2.2. Thickness and air permeability.** In order to calculate the average thickness  $\bar{z}$  of the nanofiber mat, a common relation between the basis weight  $w$ , the fiber density  $\rho_f$ , and the porosity  $p$  is used (Kwankhao et al., 2013):

$$\bar{z} = \frac{w}{\rho_f (1 - p)} \quad (6)$$

The prediction of the air permeability through the nanofiber is somehow complicated. This is due to the fact that the air flow around the electrospun nanofiber is no longer in the continuum flow regime. This necessitates the use of the so-called significant slip velocity boundary condition at the fiber surface. Therefore, the air permeability equation is developed from the model of Hosseini and Tafreshi (2010) in which the effect of slip flow on the air permeability is taken into account. The air permeability is given by the following expression:

$$AP = \frac{3 d_f^2 \Delta p}{80 \alpha \mu_{air} \bar{z}} [-\ln(\alpha) - 0.931] C_r \quad (7)$$

where  $\alpha$  is the solidity ( $1-p$ ) of the nano-fibrous web,  $C_r$  is the correction factor that is used to modify the original permeability that is based on the no-slip boundary condition in order to incorporate the slip effect, and  $\Delta p$  is the standard pressure drop for testing fabric (124.5 Pa).  $C_r$  is basically the ratio of the pressure drop when considering the no-slip boundary condition to the pressure drop across a conventional no-slip boundary condition. Thus  $C_r$  is given by the following equation:

$$C_r = \frac{ku (1 + 1.966 Kn_f)}{Ku + 1.996 Kn_f (-0.5 \ln \alpha - 0.25 + 0.25 \alpha^2)} \quad (8)$$

where  $ku$  is the Kuwabara number ( $ku = -0.5 \ln \alpha - 0.75 + \alpha - 0.25 \alpha^2$ ) and  $Kn_f$  is the fiber Kundsen number defined as the ratio of the air molecules mean free path and the fiber diameter ( $kn_f = 2\lambda/d_f$ ).

**2.1.2.3. Air filtration model.** It is based on the calculation of the filtration efficiency  $\eta$ , of a filter with a solidity  $\alpha$ , fiber diameter  $d_f$ , and thickness  $\bar{z}$ . The model begins by the calculation of the single fiber efficiency  $\eta_\Sigma$  represented as a sum of efficiencies due to diffusion  $\eta_D$ , interception  $\eta_R$ , impaction  $\eta_I$  and a combination term  $\eta_{DR}$  as follows (Kirsh et al., 1975):

$$\begin{aligned} \eta_{\Sigma} = & \eta_D + \eta_R + \eta_I + \eta_{DR} = 2.7Pe^{-2/3}(1 + 0.39ku^{-1/3}Pe^{1/3}kn_f) + 0.624Pe^{-1} + \\ & \frac{1}{2ku} \left\{ \frac{1}{1+R} - (1+R) + 2(1+R)\ln(1+R) + \frac{2.86kn_f(2+R)R}{1+R} \right\} + \frac{Stk^2}{(1+0.55Stk^2)} + \\ & 1.24ku^{-1/2}Pe^{-1/2}R^{2/3} \end{aligned} \quad (9)$$

where  $Pe$  is the Peclet number which is the ratio of advective to diffusive transport rate of aerosol particles,  $ku$  is the Kuwabara number,  $kn_f$  is the fiber Kundsen number,  $R$  is the interception number calculated as the ratio of particle diameter over the fiber diameter ( $R = d_p/d_f$ ) and  $Stk$  is the Stokes number defined as the ratio of the characteristic time of a particle to the characteristic time of the flow where it is suspended. The Peclet and Stokes number are given respectively by the following equation:

$$Pe = \frac{3\pi\mu_{air} u_0 d_p d_f}{k_b T C_c} \quad (10a)$$

$$Stk = \frac{u_0 \rho_p d_p^2 C_c}{9\mu_{air} d_f} \quad (10b)$$

where  $u_0$ ,  $d_p$ ,  $\rho_p$ ,  $k_b$ , and  $T$  are the filter face velocity, particle diameter and density, Boltzmann's constant ( $1.38 \times 10^{-23}$  J/K), and temperature, respectively.  $C_c$  is the Cunningham slip correction factor, which depends on the ratio of the mean free path of air molecules to the particle diameter and it is the result of the slip flow of the fluid at the surface (Kim, Mulholland, Kulkuck, & Pui, 2005).

Based on the single fiber collection efficiency  $\eta_{\Sigma}$ , the fiber diameter  $d_f$ , the filter thickness  $\bar{z}$ , and the filter solidity  $\alpha$ , the filter efficiency  $\eta$  is given by the following equation of Hill et al. (2013):

$$\eta = 1 - \exp\left(\frac{-4\alpha\eta_{\Sigma}\bar{z}}{\pi d_f}\right) \quad (11)$$

## 2.2. Experimental approach

### 2.2.1. Electrospinning

The electrospinning experimental approach in this study is similar to that presented recently (Ismail et al., 2016) and is shown in Fig. 2. Polymer fibers were produced by electrospinning a solution of PAN (average molecular weight of 150,000 g/mol) and N, N-dimethylformamide (DMF) ( $\geq 99.8\%$ , A.C.S. spectrophotometric grade) purchased from Sigma-Aldrich. PAN polymer is solutions were prepared by dissolving PAN powder in DMF under constant magnetic stirring for 24 h and sonicated in Cole-permer 8851 sonication bath for about 20 min prior to electrospinning process. A laboratory scale electrospinning machine (FLUIDNATEK LE-10, BIOINICIA, Spain) was used with inner and outer diameters of spinneret nozzle of 0.6 mm, and 0.9 mm, respectively. By specifying the flow rate, applied voltage (0–30 kV), the tip-to-collector distance, and the velocity of the collector drum, a horizontal electric field was generated between the nozzle and the collector. This electric field allowed the jet to leave the nozzle and to be stretched horizontally. The electrospun nanofibers were collected onto a rotating collector (100 mm diameter  $\times$  200 mm length) at room temperature of 20 °C under dry conditions (relative humidity less than 30%) similar to conditions reported by Park and Kim (2004). The rotating drum is covered by a nylon mesh of high porosity (85%) and a thickness of 210 µm. The experiment is repeated several

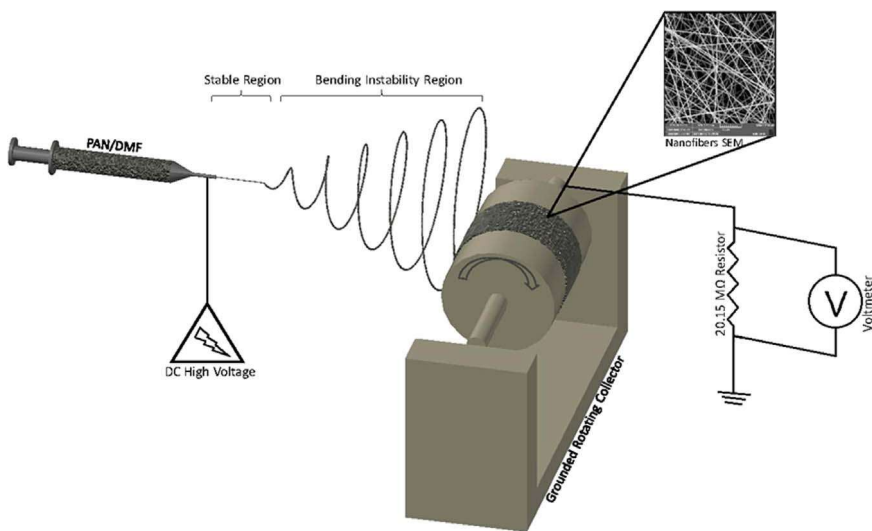


**Fig. 2.** Schematic of the electrospinning experiment (Ismail et al., 2016).

times for different processing parameters and durations to generate different nano-fibrous web properties.

### 2.2.2. Fiber diameter and thickness measurement

The fiber diameter and thickness of the electrospun samples were measured using a Scanning Electron Microscope (MIRA 3 LMU Tescan) operating at an acceleration voltage of 15 kV, working distance of 3 mm and using an InBeam detector. The SEM images were captured at 100 $\times$  to 10,000 $\times$  depending on the observation objective. For the measurement of fiber diameter, the images were captured at 10,000 $\times$  magnification. Scale given on the magnification bar was used to measure the fiber diameter. For each sample, a number of 100 readings were taken and averaged to get the mean fiber diameter and the standard deviation. On the other hand, the examination of the nano-fibrous web thickness was somehow complex. This is due to the compression of the nano-fibrous web edge when it is cut (Boppa, 2009). One way to overcome this issue is to adopt the freeze-fracturing technique which consists of cutting the web while it is immersed and frozen in liquid Nitrogen. Once the technique is implemented, the web is exposed vertically with the help of a vertical holder in the SEM machine and sputter coated with gold for 90 s using a sputter current of 10 mA (Q150T ES Turbo-Pumped Sputter Coater/Carbon Coater, Quorum Technologies). Fifty readings were taken from several places and averaged to get the mean nano-fibrous web thickness. Because the thickness measurement of the nano-fibrous web was critical and influential on the porosity measurement, an additional method was used to ensure the validity of the nano-fibrous web thickness measurement. This measurement was done using Brunswick Instrument TMS-1 gage equipped with MP-1 Metrology Processor with a thickness measurement resolution of 0.2  $\mu\text{m}$ . This experiment was repeated for 45 different locations of the electrospun nano-fibrous web. Good agreement was found between the SEM and TMS-1 gage measurements. Table 1 summarizes the SEM results for different electrospinning processing parameters. The table presents the number of readings, the minimum, maximum and mean value of the fiber diameter as well as the standard deviation. Fig. 3 shows an example of the SEM measurements of (a) the fiber diameter and (b) the nano-fibrous web thickness at electrospinning parameters of  $Q = 900 \mu\text{l/h}$ ,  $E = 97,222 \text{ V/m}$ ,  $C = 10\%$  and  $t_e = 6 \text{ h}$ .

### 2.2.3. Porosity measurement

In order to measure the porosity of the electrospun nano-fibrous web, XS Microbalance (Mettler Toledo) is used (Choi, Yang, Bae, & Jung, 2015). The mass of a unit squared centimeter area (the basis area  $w$ ) was measured. Thirty samples were chosen to be weighted from different locations of the nano-fibrous web and the average basis area  $\bar{w}$  was found. By computing the volume of the weighed sample ( $V = \bar{w}^*z$ ), the bulk density  $\rho_b$  is deduced. Therefore, the porosity,  $p$ , is computed as a function of bulk density,  $\rho_b$ , and fiber density  $\rho_f$  and is given by (Ma et al., 2005):

$$p = \left(1 - \frac{\rho_b}{\rho_f}\right) \quad (12)$$

### 2.2.4. Air permeability

A capillary flow porometer (CFP-1100 AH, American PMI) was used to measure the Frazier air permeability. For the air permeability analysis, nine different circular samples ( $D = 2.32 \text{ cm}$ ) from each web were cut from different locations. The capillary flow porometer measures the air flow rate that passes through the nano-fibrous web (Hsiao, Huang, Liu, Kuo, & Chen, 2011) and calculates the Frazier air permeability at a pressure of 125 Pa (12.7 mm  $H_2O$ ) for each sample.

**Table 1**  
SEM results of the fiber diameter measurement at different processing parameters.

Case	C (%)	E (V/m)	Q ( $\mu\text{l/h}$ )	Number of readings	Minimum value (nm)	Maximum value (nm)	Mean value (nm)	Standard deviation (nm)
1	10	97222.22	900	100	280	420	331	28
2	10	97222.22	1000	101	260	410	345	31
3	10	97222.22	1100	102	275	450	354	31
4	10	97222.22	1200	100	297	447	362	33
5	10	97222.22	1300	101	265	460	374	37
6	10	91666.67	900	100	263	415	345	34
7	10	102777.78	900	100	260	414	321	31
8	10	108333.33	900	103	263	405	311	32
9	10	113888.89	900	103	270	410	304	35
10	8	97222.22	900	100	268	416	324	30
11	9	97222.22	900	101	278	415	330	33
12	11	97222.22	900	100	275	413	334	37
13	10	88888.89	1000	100	264	455	359	29
14	10	94444.44	1000	100	260	458	351	36
15	10	100000	1000	101	341	443	340	32
16	10	105555.56	1000	105	260	418	324	35
17	10	111111.11	1000	102	265	411	319	30
18	8	97222.22	1000	101	339	445	340	31
19	9	97222.22	1000	100	269	413	344	34
20	11	97222.22	1000	101	270	405	345	39

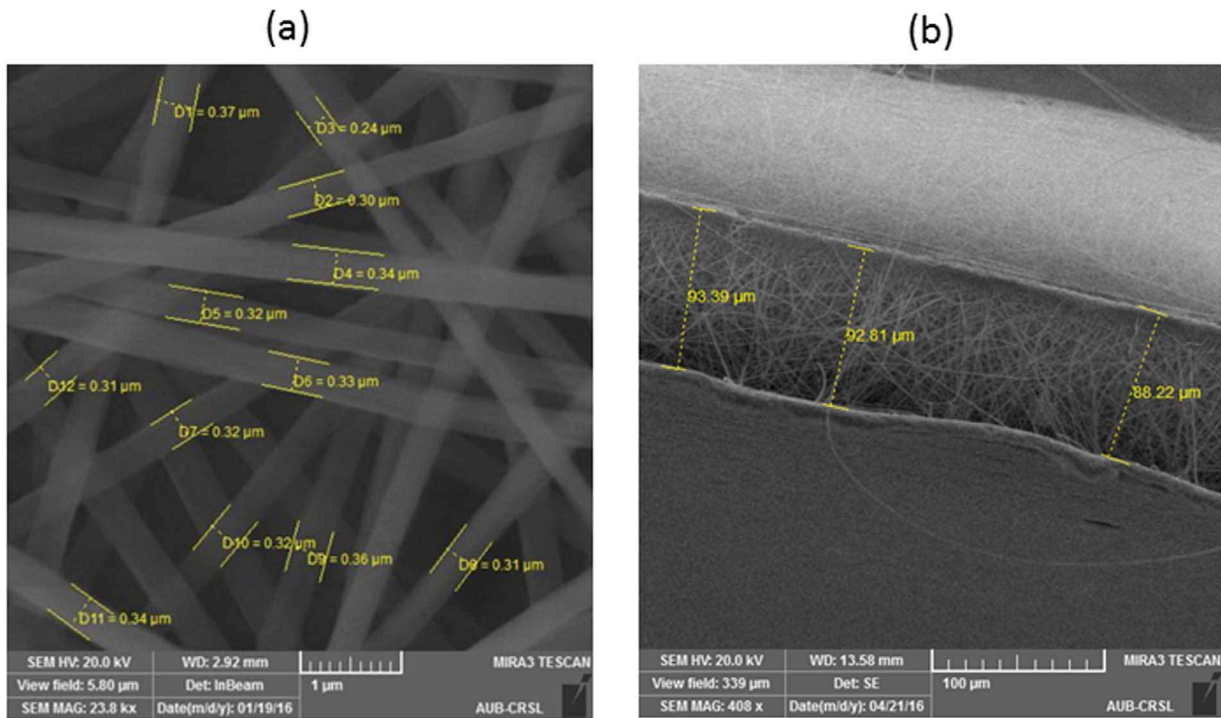


Fig. 3. SEM images of nano-fibrous web obtained for the following processing parameters ( $Q = 900 \mu\text{l/h}$ ,  $E = 97,222 \text{ V/m}$ ,  $C = 10\%$  and  $t_e = 6 \text{ h}$ ) showing the measurement of (a) fiber diameter (b) nano-fibrous web thickness.

#### 2.2.5. Air filtration (aerosol collection efficiency)

A schematic diagram of the experimental set up used for the air filtration efficiency measurement is illustrated in Fig. 4(a). The system consists of a condensation aerosol generator, an injector, a filter holder, a sampling instrument, a flow controller and a diaphragm pump. Some instruments photos are shown in Fig. 4(b). The experiment was performed in a small wind tunnel with a cross section of  $15 \times 15 \text{ cm}$  and  $1 \text{ m}$  length. The wind tunnel fan is used for mixing purpose. The condensation aerosol generator was used to produce poly-disperse aerosol particles of concentration greater than  $10^6 \text{ particles/cm}^3$  in a diameter range of  $0.3\text{--}1 \mu\text{m}$ . The generated aerosol particles are injected into the wind tunnel using five injection ports of  $1 \text{ cm}$  diameter close to the wind tunnel fan.

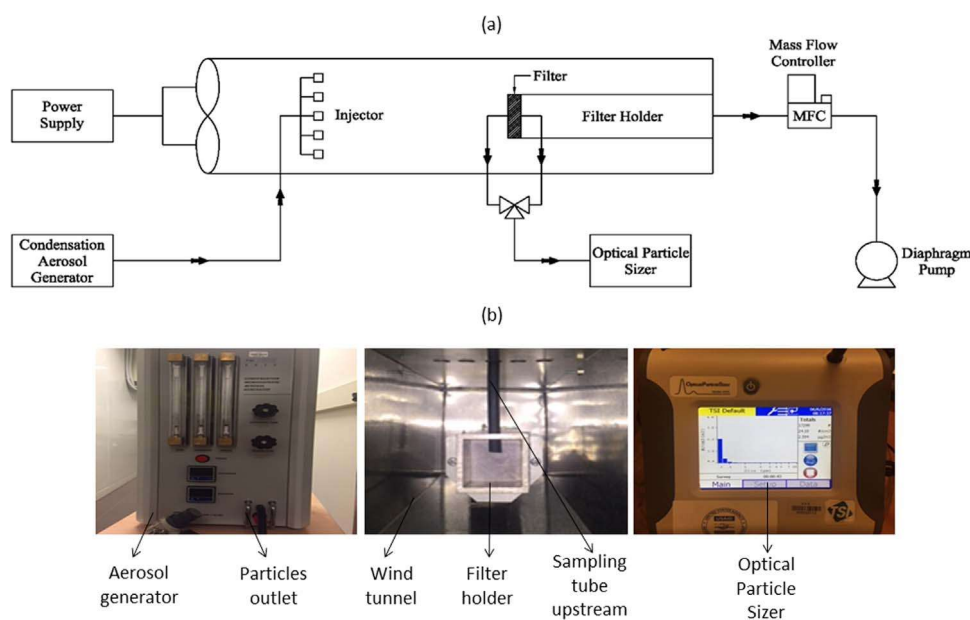


Fig. 4. (a) A schematic diagram of the experiment and (b) the devices used in the filtration experiment.

The particles were then carried to the filter holder by the wind. The filter holder is a 5 cm × 5 cm cross section channel and 40 cm length placed at the end of the wind tunnel. The flow controller (0–5 l/min) and the diaphragm pump (2–5 l/min) are used to generate the desirable face velocity. Particle concentrations were measured upstream and downstream using an optical particle sizer of a fast-response and high size resolution. Finally, the aerosol filtration efficiency  $\eta$  of the electrospun nano-fibrous web is given by the following equation:

$$\eta = (C_u - C_d)/C_u \quad (13)$$

where  $C_u$  and  $C_d$  are the upstream and downstream concentration of the electrospun nano-fibrous web respectively.

### 3. Results and discussions

PAN solutions at various concentrations were electrospun under the ambient conditions of 20 °C and a relative humidity of about 30%. A set of experiments was performed where the flow rate was varied from 900 to 1320 µl/h, the electric field was varied from 90 to 120 kV/m, the solution concentration was varied from 8% to 11% and the time of electrospinning was varied from 10 to 360 min. The electrospinning parameters are chosen in a range that ensures the generation of a continuous jet without droplets. This range is reported in the literature by Barua and Saha (2015) and are used in the previous published paper of Ismail et al. (2016). The effect of each processing parameter on the morphology of the nano-fibrous web as well as the air filtration efficiency is studied by varying one parameter and holding all the other constants at the following values:

$$Q = 900 \mu\text{l}/\text{hr}; E = 98 \text{ kV/m}; C = 10\%, \text{ and } te = 10 \text{ min}, u_0 = 5 \text{ cm/s}, d_p = 300 \text{ nm}.$$

#### 3.1. Effect of processing parameters on thickness and porosity

##### 3.1.1. Electrospinning time

Fig. 5 shows the variation of the nano-fibrous web porosity and thickness as a function of the electrospinning time as measured experimentally and predicted by the modeling approach. As shown in Fig. 5, the electrospinning time affects both the thickness and the porosity of the nano-fibrous web. Good agreement is found between the theoretical and the experimental values with a relative error less than 8%. The number of layers forming the nano-fibrous web increases by increasing the electrospinning time. As these layers are randomly deposited, the fibers of a layer may block the pores of the previous deposited layer. Thus, the porosity of the nanofiber decreases gradually by deposition time. These findings agree with those reported in the literature by Givehchi, Li, and Tan (2016).

##### 3.1.2. Processing parameters of electrospinning ( $Q$ , $E$ , $C$ )

Fig. 6 shows the effect of processing parameters on the morphology of the nano-fibrous web as measured experimentally and predicted by the models. It illustrates the influence of varying (a) the volumetric flow rate, (b) the electric field, and (c) the polymer concentration of electrospinning, respectively, on both porosity and thickness. Good agreement is observed between the theoretical and the experimental values with a relative error less than 8%. As was reported in the previous study of Ismail et al. (2016), the final fiber diameter increases by increasing the flow rate and the polymer concentration and decreases by increasing the electric field. Therefore, the effect of electrospinning parameters on the porosity and thickness of the nano-fibrous web is directly attributed to the effect of the final fiber diameter on them. Fig. 7 presents the effect of the electrospinning fiber diameter on the porosity and thickness determined by the developed model. It is clear that increasing the fiber diameter causes larger pore size as was reported in the literature (Kwankhao et al., 2013). One would expect that increasing the fiber diameter would lead intuitively to an increase of porosity. However, the porosity is slightly changed (increased/ decreased) with the increase in the fiber diameter (see Fig. 7). The

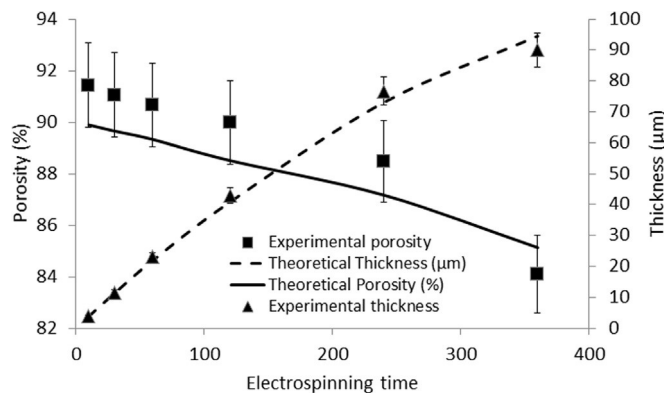


Fig. 5. Effect of electrospinning time on the porosity and thickness of the nano-fibrous web for the following processing parameters ( $Q = 900 \mu\text{l}/\text{h}$ ,  $E = 97,222 \text{ V/m}$ , and  $C = 10\%$ ).

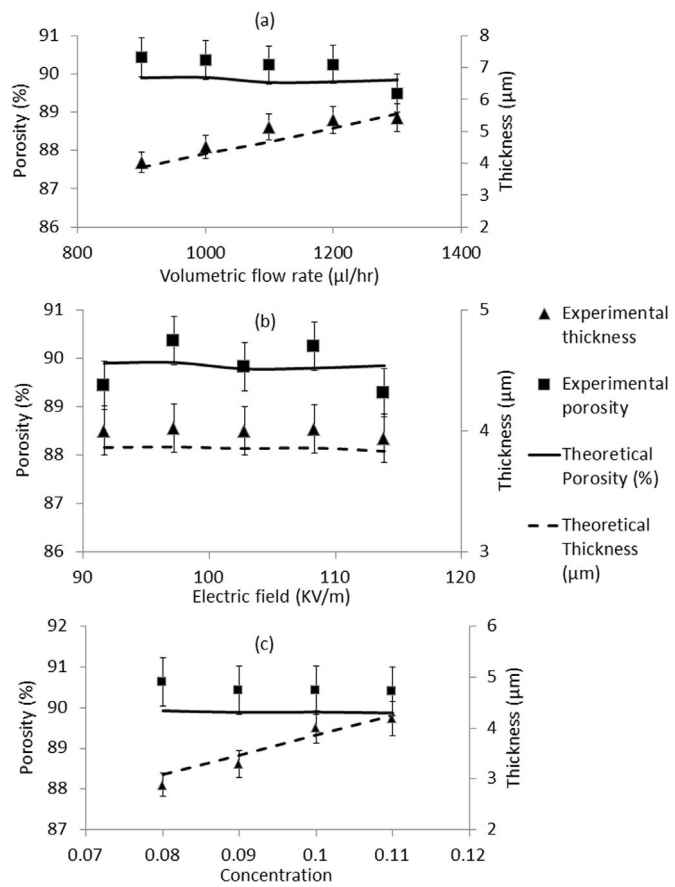


Fig. 6. Effect of (a) flow rate (b) electric field (c) concentration on porosity and thickness at the nano-fibrous web at an electrospinning time of 10 min.

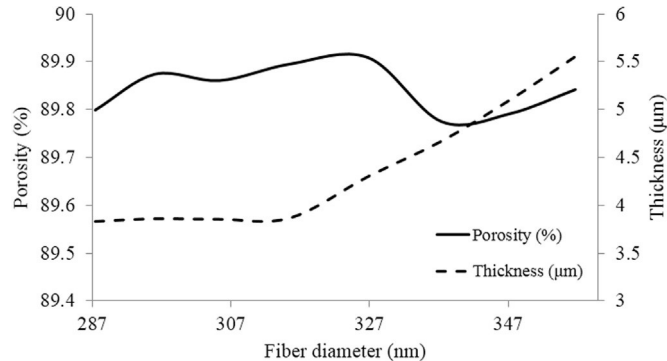


Fig. 7. Effect of the electrospun fiber diameter on predicted nano-fibrous web thickness and porosity.

main reason for this behavior is that the porosity is also affected by the change in the nano-fibrous web thickness. Indeed, porosity and thickness are inversely correlated; if the thickness increases, the porosity decreases and vice versa. As was shown in Fig. 7, the thickness is increasing with the fiber diameter. Thus, the porosity is dominated by two opposite phenomena as a consequence of the fiber diameter increase; increasing the pore size and increasing the thickness. The former leads to an increase in porosity while the latter does the opposite. This dual effect is the cause of the slight change of the porosity as a function of the final fiber diameter.

### 3.2. Effect of processing parameters on air permeability and aerosol filtration

#### 3.2.1. Electrospinning time

Fig. 8 illustrates the effect of the electrospinning time on the air permeability and the air filtration efficiency against aerosol particles for the following processing parameters ( $Q = 900 \mu\text{l/h}$ ,  $E = 97,222 \text{ V/m}$ , and  $C = 10\%$ ). The experimental results are in a

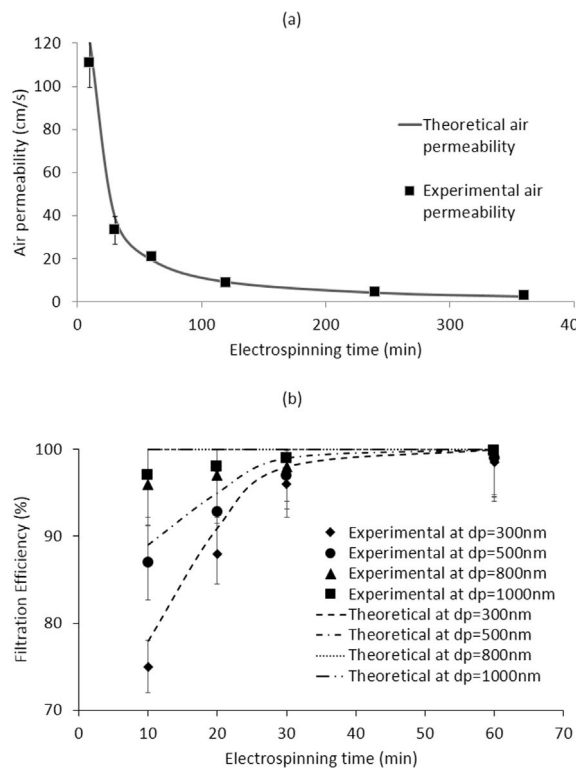


**Fig. 8.** Effect of electrospinning time on (a) air permeability (b) aerosol filtration for different particle diameters ( $dp$ ) for the following processing parameters ( $Q = 900 \mu\text{l}/\text{h}$ ,  $E = 97,222 \text{ V/m}$ ,  $C = 10\%$ ).

good agreement with the theoretical findings (i.e., the maximum and the average relative error are respectively 10% and 7%). Fig. 8(a) shows that the air permeability is decreasing significantly as the coating time increases. Only 20 min of electrospinning is able to decrease the air permeability from 120 to 40 cm/s. The air permeability is strongly related to the thickness and porosity of the nano-fibrous web. As the coating time increases, the thickness increases while the porosity decreases (see Fig. 6). This contributes to a large resistance to the air flow leading to a significant decrease of air permeability. These findings are also reported by Faccini et al. (2012).

Fig. 8(b) shows the results obtained for the penetration of nanoparticles (size range of 300–1000 nm) through the nano-fibrous web deposited on the nylon screen mesh as a function of different electrospinning time at a velocity of 5 cm/s. The electrospinning time range is limited in this figure to 60 min because both simulations and experiments prove that, after this time, the filtration efficiency reaches 100% (i.e. no particle passes through). The results show that the predictions of the model lie in the standard deviation of the experimental data. Moreover, the results show that the filtration of aerosol particles through nano-fibrous web followed the classical filtration model: the filtration efficiency decreases when reducing the particle size, due to Brownian diffusion (Faccini et al., 2012). Therefore, in our study, the most penetrating particles were found to have a size of 300 nm. On the other hand, the filtration of aerosol particles increases with the time of electrospinning reaching an approximate total filtration (100%) after one hour of coating. This is of course due to the fact that increasing the thickness and decreasing the porosity by increasing the electrospinning time will form an efficient barrier to aerosol particles generation. The least efficient nano-fibrous web was the sample having the least coating time (10 min). Indeed, after only ten minutes of coating, the nano-fibrous web is able to filtrate more than 75% of the most penetrating particles while having a significant air permeability of 120 cm/s. By tripling the coating time to 30 min, the nano-fibrous web filtration increases harshly to about 90% for the most penetrating particles. This finding clearly proves the potential of nano-fibrous web in the development of barrier materials against aerosol particles. Fig. 8(b) shows that the aerosol filtration agrees with the experimental findings. The standard deviation of the measured values was within (2%).

### 3.2.2. Processing parameters of electrospinning ( $Q$ , $E$ , $C$ )

It is of interest to study the effect of the electrospinning processing parameters ( $Q$ ,  $E$ ,  $t_e$ ) on the air permeability and the filtration efficiency of the nano-fibrous web. The chosen nano-fibrous web corresponds to an electrospinning time of 10 min. The particle diameter studied in the filtration efficiency is the most penetrating particle found (300 nm) at a wind velocity of 5 cm/s. It is shown that when the flow rate increases (see Fig. 9(a)), the air permeability decreases while the filtration efficiency increases. The same results are found when the electric field or the concentration increases (see Fig. 9(b-c)). Although the flow rate and the concentration variation have the opposite effect of the electric field on the fiber diameter of electrospinning (Ismail et al., 2016), they all affect the air permeability and the filtration efficiency in the same way.

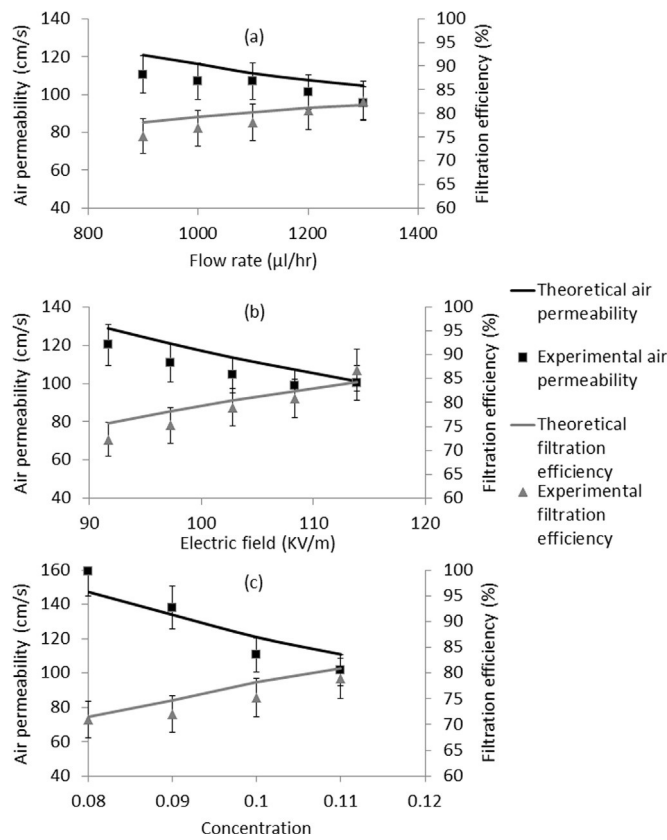


Fig. 9. Effect of (a) flow rate (b) electric field (c) concentration on air permeability and filtration efficiency at an electrospinning time of 10 min.

It is important to see the effect of fiber diameter on the air permeability and the filtration efficiency of the nano-fibrous web chosen (10 min of coating time) at the most penetrating aerosol particle (300 nm) and at a velocity of 5 cm/s. As seen in Fig. 10, the predicted air permeability and the filtration efficiency experience a maximum and a minimum respectively for the same fiber diameter 315 nm. The porosity is the ratio of the void volume over the total volume which is the sum of the volume of fibers (solid volume) and the void volume. Therefore, if the volume of fibers increases (by increasing the fiber diameter) and the porosity is constant, the volume of pores must increase. In other words, when the fiber diameter increases, the void size increases. This agrees with the findings of Matsumoto and Tanioka (2011) who reported that the average pore size between nanofibers decreased with a decrease in the fiber diameter. Moreover, the air permeability and filtration efficiency is observed to behave in an opposite manner because the air is carrying the aerosol particles. So if the air permeability is increasing, the penetration of the aerosol particles increases and the filtration efficiency must decrease. Furthermore, the air permeability profile as function of fiber diameter is related to the thickness and the porosity of the nanofiber web (see Fig. 7). As the thickness increases, the air permeability decreases. As the porosity increases, the air permeability increases. Therefore, in order to explain the behavior shown in Fig. 10, the analysis is

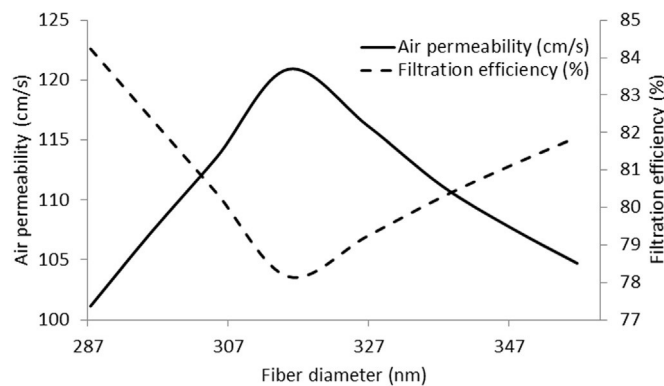


Fig. 10. Effect of the electrospun fiber diameter on predicted nano-fibrous web air permeability and filtration efficiency.

separated into two parts: the first part for  $d_f < 315$  nm, and second part for  $d_f > 315$  nm. In the first part, it is shown that the air permeability increases and the filtration efficiency decreases with the fiber diameter. Referring to Fig. 7, the porosity and the thickness are slightly changed for  $d_f < 315$  nm. However, the fiber diameter is increasing; thus, the pore volume must increase to conserve the porosity. Any increase in pore size will evidently increase the air permeability and decrease the filtration efficiency. In the second part, it is shown that the air permeability decreases and the filtration efficiency increases with the fiber diameter. Referring to Fig. 7, the porosity stays unchanged while the thickness increases significantly for  $d_f > 315$  nm. The increase in thickness will result in an increase in air permeability and a decrease of filtration efficiency.

#### 4. Design charts correlation

Design charts are developed by performing many simulations (180 simulations) on the combined model to establish the relation between the nano-fibrous web filtration performance or its air permeability and the electrospinning processing parameters.

The first design chart is Fig. 11(a-b) which presents the fiber diameter as a function of the electrospinning processing parameters ( $Q, E$ ) at two different concentrations of (a) 8% and (b) 10%. These design charts could be interpolated to obtain the fiber diameter at the following range of concentrations of 8–11%. The lower limit provides the continuity of the jet while the upper limit is due to the use of the electrospinning model (Ismail et al., 2016) based on the assumption that at the final stage of electrospinning, the competition is between the surface tension and the electrostatic force. This assumption is not applied to relatively high polymer solution concentration ( $\geq 12\%$ ) because the relatively large viscous force in this case prevents reaching the final stage of bending instabilities. On the other hand, the electrospinning parameters (flow rate and electric field) are chosen in a range to generate a continuous jet without droplets so that the conservation equations are verified (Barua & Saha, 2015). The second design chart is Fig. 12 which shows the ratio of the porosity over the thickness as a function of the fiber diameter for different electrospinning time. The last design chart is Fig. 13 which shows the air permeability and the air filtration for the nano-fibrous web as function of the porosity/thickness and the fiber diameter.

These design charts (Figs. 11–13) are utilized in a way that makes it possible for a given input of electrospinning processing parameters ( $E, Q, C$ , and  $t_e$ ) to predict directly the filtration performance of the nano-fibrous web as well as its air permeability. In addition, the design charts allow getting the electrospinning processing parameters for desirable air permeability/ air filtration properties by going backwards from the output of the combined model of these properties to the needed input parameters.

Two examples are considered to illustrate the utilization of these design charts. The first example considers a case of a PAN solution of 10% concentration and its selection points are shown as a black circle on the design charts figures. For the following processing parameters ( $Q = 1000 \mu\text{l}/\text{h}$ ,  $E = 110 \text{ kV/m}$ ), Fig. 11(b) predicts a fiber diameter of 300 nm. From Fig. 12, after a deposition time of 30 min, for a fiber diameter of 300 nm, the ratio of porosity over the thickness is about 8%/ $\mu\text{m}$ . For the obtained porosity over thickness, and for the same fiber diameter, Fig. 13 indicates that the air permeability is 38 cm/s and the air filtration for the most penetrating particles is 98%. In the second example, consider the case where the desirable air permeability is 100 cm/s and

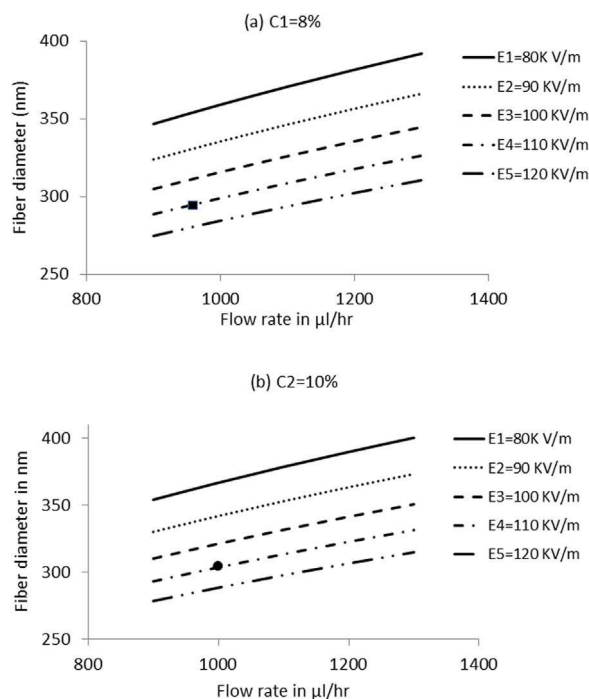
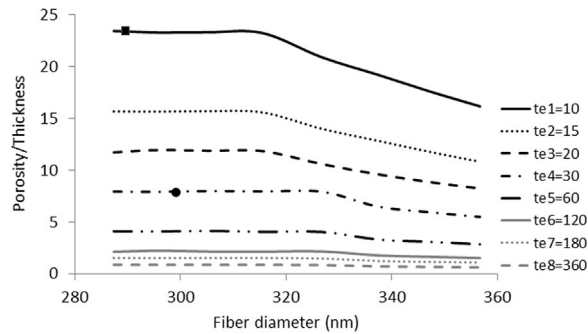
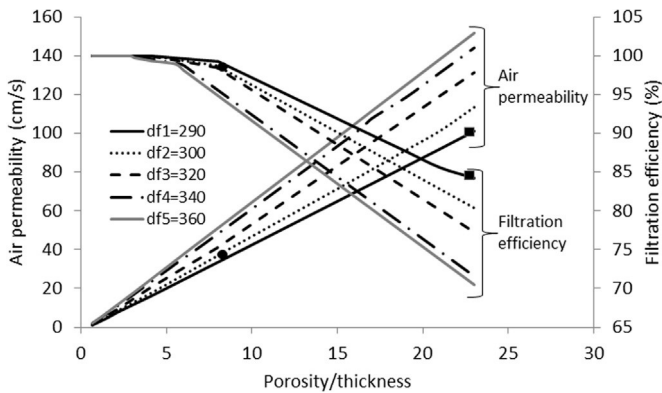


Fig. 11. Design chart of the fiber diameter as function of flow rate and electric field at polymer concentration of (a)  $C = 8\%$  and (b)  $C = 10\%$ .



**Fig. 12.** Design chart of the porosity over the thickness as function of fiber diameter for different time of electrospinning.



**Fig. 13.** Design chart of the air permeability and filtration efficiency as function of porosity over thickness at different fiber diameters.

its selection points are designates as a black square on the design charts figures. Fig. 13 shows that for this air permeability, we can choose different fiber diameter. In order to have a maximum filtration, it is worth to choose the fiber diameter of 290 nm (filtration efficiency of 85%). For these parameters, the ratio of porosity to thickness is 23%/μm. From Fig. 12, for 290 nm fiber diameter and a ratio of porosity to thickness of 23%/μm, the time of electrospinning is 10 min. In order to obtain the electrospinning processing parameters, at a concentration of 8% for example, Fig. 11(a) shows that the electric field is 110 kV/m, and a flow rate of 980 μl/h. It is of interest to state that, although the design charts give us the ratio of porosity over thickness, however, these two morphological properties could be predicted separately using Eq. (6).

## 5. Conclusion

In this study, a systematic model that relates the electrospinning processing parameters to the morphological properties and the filtration efficiency of the nano-fibrous web was developed. The systematic model was validated at each step with experiments. The results showed that the air permeability diminishes when the coating time of electrospinning increases. However, the filtration efficiency increases to reach a complete filtration after one hour of coating. On the other hand, it is shown that the air permeability and the filtration efficiency experience a maximum and a minimum respectively for the same fiber diameter. The reason is that as the fiber diameter increases to this fiber diameter value, the volume of pores increases to conserve a constant porosity leading to an increase in air permeability and a decrease in filtration efficiency. Beyond this fiber diameter value, the volume of pores is compensated by the increase of thickness that leads to a decrease in air permeability and increase in filtration efficiency. Finally, the study presents an engineering tool (design charts) that allow the determination of the desired air permeability and the filtration performance of the nano-fibrous web from the electrospinning parameters and vice versa within a wide range of feasible processing parameters and fiber diameters.

## Acknowledgment

The authors would like to acknowledge the financial support of the Lebanese National Council for Scientific Research for the project Award number 103061-22909.

## References

- Abuzade, R. A., Zadhouh, A., & Gharehaghaji, A. A. (2012). Air permeability of electrospun polyacrylonitrile nanoweb. *Journal of Applied Polymer Science*, 126(1),

- 232–243.
- Ballengee, J. B., & Pintauro, P. N. (2011). Morphological control of electrospun Nafion nanofiber mats. *Journal of the Electrochemical Society*, 158(5), 568–B572.
- Barua, B., & Saha, M. C. (2015). Investigation on jet stability, fiber diameter, and tensile properties of electrospun polyacrylonitrile nanofibrous yarns. *Journal of Applied Polymer Science*, 132, 18.
- Barhate, R. S., & Ramakrishna, S. (2007). Nanofibrous filtering media: filtration problems and solutions from tiny materials. *Journal of Membrane Science*, 296(1), 1–8.
- Bhattacharjee, P. K., Schneider, T. M., Brenner, M. P., McKinley, G. H., & Rutledge, G. C. (2010). On the measured current in electrospinning. *Journal of Applied Physics*, 107(4), 044306.
- Boppa, V. (2009). Characterization of structure and tensile properties of electrospun web.
- Chattopadhyay, S., Hatton, T. A., & Rutledge, G. C. (2015). Aerosol filtration using electrospun cellulose acetate fibers. *Journal of Materials Science*, 51(1), 204–217.
- Choi, J., Yang, B. J., Bae, G.-N., & Jung, J. H. (2015). Herbal extract incorporated nanofiber fabricated by an electrospinning technique and its application to antimicrobial air filtration. *Interfaces ACS Applied Materials & Interfaces*, 7(45), 25313–25320.
- Davies, C. N. (1973). *Air Filtration*. Academic Press.
- Faccini, M., Vaquero, C., & Amantia, D. (2012). Development of protective clothing against nanoparticle based on electrospun nanofibers. *Journal of Nanomaterials*, 2012, 1–9.
- Fang, J., Wang, X., & Li, T. (2011). Functional applications of electrospun nanofibers. *Nanofibers – Production, Properties and Functional Applications*.
- Feng, J. (2002). The stretching of an electrified non-Newtonian jet: A model for electrospinning. *Physics of Fluids*, 14, 3912–3926.
- Fridrikh, S. V., Jian, H. Y., Brenner, M. P., & Rutledge, G. C. (2003). Controlling the fiber diameter during electrospinning. *Physical Review Letters*, 90(14), 144502.
- Givehchi, R., Li, Q., & Tan, Z. (2016). Quality factors of PVA nano-fibrous filters for airborne particles in the size range of 10–125 nm. *Fuel*, 181, 1273–1280.
- Haines, A., Kovats, R., Campbell-Lendrum, D., & Corvalan, C. (2006). Climate change and human health: Impacts, vulnerability and public health. *Public Health*, 120(7), 585–596.
- Hill, M. A., Ghee, T. A., Kaufman, J., & Dhaniyala, S. (2013). Investigation of aerosol penetration through individual protective equipment in elevated wind conditions. *Aerosol Science and Technology*, 47(7), 705–713.
- Hohman, M. M., Shin, M., Rutledge, G., & Brenner, M. P. (2001). Electrospinning and electrically forced jets. i. stability theory. *Physics of Fluids*, 13(8), 2201–2220.
- Hosseini, S., & Tafreshi, H. V. (2010). Modeling permeability of 3-D nanofiber media in slip flow regime. *Chemical Engineering Science*, 65(6), 2249–2254.
- Hsiao, H.-Y., Huang, C.-M., Liu, Y.-Y., Kuo, Y.-C., & Chen, H. (2011). Effect of air blowing on the morphology and nanofiber properties of blowing-assisted electrospun polycarbonates. *Journal of Applied Polymer Science*.
- Huang, Z.-M., Zhang, Y.-Z., Kotaki, M., & Ramakrishna, S. (2003). A review on polymer nanofibers by electrospinning and their applications in nanocomposites. *Composites Science and Technology*, 63(15), 2223–2253.
- Ismail, N., Maksood, F. J., Ghaddar, N., Ghali, K., & Tehrani, A. B. (2016). Simplified modeling of the electrospinning process from stable jet region to unstable region to predict final nano-fiber diameter. *Journal of Applied Polymer Science*, 133(43), 44112.
- Kim, J., Mulholland, G., Kukuck, S., & Pui, D. (2005). Slip correction measurements of certified PSL nanoparticles using a nanometer differential mobility analyzer (nano-DMA) for Knudsen number from 0.5 to 83. *Journal of Research of the National Institute of Standards and Technology*, 110(1), 31.
- Kirsh, A., Stechkina, I., & Fuchs, N. (1975). Efficiency of aerosol filters made of ultrafine polydisperse fibres. *Journal of Aerosol Science*, 6(2), 119–124.
- Kuo, Y.-Y., Bruno, F. C., & Wang, J. (2014). Filtration performance against nanoparticles by electrospun nylon-6 media containing ultrathin nanofibers. *Aerosol Science and Technology*, 48(12), 1332–1344.
- Kwankhao, B., Ulbricht, M., & Gutmann, J. (2013). Microfiltration membranes via electrospinning of polyethersulfone solutions.
- Lee, S., & Obendorf, S. K. (2007). Use of electrospun nanofiber web for protective textile materials as barriers to liquid penetration. *Textile Research Journal*, 77(9), 696–702.
- Leung, W. W.-F., Hung, C.-H., & Yuen, P.-T. (2010). Effect of face velocity, nanofiber packing density and thickness on filtration performance of filters with nanofibers coated on a substrate. *Separation and Purification Technology*, 71(1), 30–37.
- Lowery, J. L. (2009). Characterization and modification of porosity in electrospun polymeric materials for tissue engineering applications. PhD Diss. Massachusetts Institute of Technology.
- Ma, Z., Kotaki, M., Yong, T., He, W., & Ramakrishna, S. (2005). Surface engineering of electrospun polyethylene terephthalate (PET) nanofibers towards development of a new material for blood vessel engineering. *Biomaterials*, 26(15), 2527–2536.
- Matsumoto, H., & Tanioka, A. (2011). Functionality in electrospun nanofibrous membranes based on fiber's size, surface area, and molecular orientation. *Membranes*, 1(3), 249–264.
- Pai, C.-L., Boyce, M. C., & Rutledge, G. C. (2011). On the importance of fiber curvature to the elastic moduli of electrospun nonwoven fiber meshes. *Polymer*, 52(26), 6126–6133.
- Park, M. S., & Kim, J. K. (2004). Breath figure patterns prepared by spin coating in a dry environment. *Langmuir*, 20(13), 5347–5352.
- Shin, Y. M., Hohman, M. M., Brenner, M. P., & Rutledge, G. C. (2001). Electrospinning: A whipping fluid jet generates submicron polymer fibers. *Applied Physics Letters*, 78(8), 1149.
- Tafreshi, H. V., Rahman, M. A., Jaganathan, S., Wang, Q., & Pourdeyhimi, B. (2009). Analytical expressions for predicting permeability of bimodal fibrous porous media. *Chemical Engineering Science*, 64(6), 1154–1159.
- Taylor, G. (1969). Electrically Driven Jets. Proceedings of the Royal Society of London. A. Mathematical and Physical Sciences, 313, 453–475.
- Wang, Q., Maze, B., Tafreshi, H. V., & Pourdeyhimi, B. (2007). Simulating through-plane permeability of fibrous materials with different fiber lengths. *Modelling and Simulation in Materials Science and Engineering*, 15(8), 855–868.
- Yarin, A. L. (2011). Coaxial electrospinning and emulsion electrospinning of core-shell fibers. *Polymer Advanced Technology*, 22(3), 310–317.
- Yun, K. M., Hogan, Jr. C. J., Matsubayashi, Y., Kawabe, M., Iskandar, F., & Okuyama, K. (2007). Nanoparticle filtration by electrospun polymer fibers. *Chemical Engineering Science*, 62, 4751.